Nonlinear Bloch dynamics and spin-wave generation in a Bose-Hubbard ladder subject to effective magnetic field

Ai-Xia Zhang,* Wei Zhang, Ya-Hui Qin, Xiao-Wen Hu, Xin Qiao, and Ju-Kui Xue†
College of Physics and Electronic Engineering, Northwest Normal University, Lanzhou, 730070, China

(Received 17 August 2022; accepted 12 October 2022; published 28 October 2022)

The two-leg magnetic ladder is the simplest and ideal model to reflect the coupling effects of lattice and magnetic field. It is of great significance to study some novel phases, topological characteristics, and chiral characteristics in condensed matter physics. In particular, the left-right leg degree of freedom can be regarded as a pseudospin, and the two-leg magnetic ladder also provides an ideal platform for the study of spin dynamics. Here the ground state, Bloch oscillations (BOs), and spin dynamics of the interacting two-leg magnetic ladder subject to an external linear force are studied by using variational approach and numerical simulation. In the absence of the external linear force, the critical condition of transition between the zero-momentum state and plane-wave state is obtained analytically, and the physical mechanism of the ground-state transition is revealed. When the external linear force presents, the occurrence of BOs excites the spin dynamics, and we reveal the chiral BOs and the accompanied spin dynamics of the system in different ground states. In particular, we further study the influence of periodically modulated linear force on BOs and spin dynamics. The frequencies of the linear force corresponding to the resonances and pseudoresonances are obtained analytically, which result in rich nonlinear dynamics. In resonances, stable and strong BOs (with larger amplitude) are observed. In pseudoresonances, because the pseudoresonance frequencies are related to the initial momentum and phase of the wave packet, a dispersion effect takes place and strong diffusion of wave packet occurs. When the frequency is nonresonant, drift and weak dispersion of wave packet occur simultaneously with the wave-packet oscillation. In all cases, the wave-packet dynamics is accompanied with periodic but anharmonic pseudospin oscillation. The BOs and spin dynamics are effectively controlled by periodically modulating the linear force.

DOI: 10.1103/PhysRevE.106.044215

I. INTRODUCTION

In recent years, the artificial gauge field [1] induced by the coupling between light and cold atoms (i.e., Raman coupling between the spin states of ultracold atoms), including artificial electric field [2], artificial magnetic field [3], spin-orbit coupling [4], etc., has generated a series of rich physical properties and derived some new research fields. Among them, the combination of optical lattice and artificial gauge field to realize effective magnetic field of cold atoms in optical lattice has become a hot field in cold atom physics [5–11].

The physics of cold atoms in optical lattices subject to artificial magnetic fields is a spatial high-dimensional problem that poses challenges to theoretical studies. In recent years, more attention has been paid to pure and highly controllable low-dimensional nontrivial topology models. Since the one-dimensional system under the effect of magnetic field does not have the orbital effect, the ladder model with two-leg structure [12–14] has become one of the simpler ideal physical models to study the orbital magnetic field effects and lattice coupling effects in low-dimensional quantum systems. It also provides a great research environment for in-depth revealing some novel phases, topological characteristics, and chiral characteristics in condensed matter physics. Furthermore, it provides a new and effective way to explore a new method to realize spin-orbit coupling in one-dimensional quantum gas.

Experimentally, there are many ways to implement the magnetic ladder in cold atom systems. In 2014, Atala *et al.* [12] realized the bosonic ladder system of ultracold atoms in artificial gauge field by using superlattice and laser-induced tunneling technology [4,15]. The current research has proved the existence of novel quantum phases including superfluid phase, Mott-insulator phase, charge density wave phase, vortex density wave phase, biased ladder phase, etc. [16–21]. In addition to the complex phase transition process, the two-leg magnetic ladder system has abundant dynamic characteristics. In actual experiments, due to the existence of magnetic field gradient and gravity, the ladder tends to tilt, and the condensate propagates through directed center-of-mass motion, which leads to a series of rich and interesting quantum phenomena, such as chiral Landau Zener tunneling, Bloch oscillation, localization, coherent transformation, superfluid characteristics, etc. [22–30]. When a harmonic confinement potential is applied, the critical slowing down in the collective mode dynamics of the two-leg magnetic ladder system is also found [25]. More interestingly, the characteristics of these rich dynamic phenomena can be used to visually distinguish the phases of the system. Obviously, the study of dynamics phenomena of magnetic ladder system provides

*zhangax@nwnu.edu.cn
†xuejk@nwnu.edu.cn

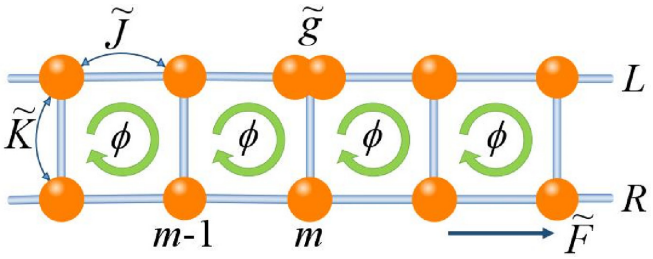

FIG. 1. The sketch of the two-leg ladder with magnetic flux.

more opportunities for exciting new dynamic phase transitions, accurately controlling and identifying particle dynamics and ground-state phase transitions of the system. However, there are still many problems to be explored in depth. Considering the atomic interaction, the competition relationship among atomic interaction, magnetic field, and rung-to-leg coupling ratio for inducing the ground-state phase transition is not clear. Especially, the nonequilibrium dynamics in different ground states under external modulation is still open subject.

In this paper, the ground state and the dynamics of the interacting bosonic ladder system subject to a synthetic magnetic field under the action of a static and periodically modulated linear force are studied analytically and numerically. In the absence of the external linear force, the ground state of the system is studied, two states, i.e., zero-momentum state and plane-wave state, are presented, and the threshold for transition of the two states are obtained analytically. The physical mechanism of ground-state transitions is revealed explicitly. In the presence of the external linear force, the Bloch oscillations (BOs) and spin dynamics initialized in different ground states are discussed. The results show that BOs exhibits the chiral characteristics and depends on the ground state. Moreover, we addressed the phenomenon of dynamic localization of Bloch wave packets subjected to a periodically modulated linear force. Rich Bloch and spin dynamics are presented, including strong BOs with larger amplitude, drift of Bloch wave packet, and significant dispersion of the wave packet. Accordingly, periodic but anharmonic spin dynamics are observed.

The paper is organized as follows. In Sec. II, we introduce the model of the two-leg ladder with an artificial magnetic field and an external linear force. In Sec. III, the ground-state transition of the system are analyzed with a variational approach, and the dispersion relation and ground-state diagram are presented in detail. In Sec. IV, the chiral BOs and corresponding spin dynamics are presented, and the influence of system parameters on BOs and spin dynamics is discussed. In Sec. V, we study the modulation of BOs, and the controllable wave-packet dynamics and spin dynamics are clearly presented. Finally, in Sec. VI, a brief summary is given.

II. THE MODEL AND VARIATIONAL APPROACH

We study the ground-state and Bloch dynamics of two-leg bosonic ladder subject to an artificial magnetic field (see Fig. 1). With a linear force $\tilde{F}$ applied along the legs and a magnetic flux ϕ piercing the each unit cell, the Hamiltonian of the interacting bosonic ladder system is [12,16,29,31–33]

$$\begin{aligned}\hat{H} = &-\tilde{J}\sum_m (e^{i\phi}\hat{a}_{m,L}\hat{a}^\dagger_{m+1,L} + e^{-i\phi}\hat{a}_{m,R}\hat{a}^\dagger_{m+1,R} + \text{H.c.}) \\ &- \tilde{K}\sum_m (\hat{a}^\dagger_{m,L}\hat{a}_{m,R} + \text{H.c.}) + \frac{\tilde{g}}{2}\sum_m (\hat{a}^\dagger_{m,L}\hat{a}^\dagger_{m,L}\hat{a}_{m,L}\hat{a}_{m,L} \\ &+ \hat{a}^\dagger_{m,R}\hat{a}^\dagger_{m,R}\hat{a}_{m,R}\hat{a}_{m,R}) + \tilde{F}\sum_m m(\hat{a}^\dagger_{m,L}\hat{a}_{m,L} + \hat{a}^\dagger_{m,R}\hat{a}_{m,R}).\end{aligned} \tag{1}$$

Here the operator $\hat{a}_{m,\sigma}$ refers to annihilating a particle at site m in the left or right leg of the ladder (corresponding to $\sigma = L$ or R). $\tilde{J}$ and $\tilde{K}$ represent the tunneling strengths along the legs and rungs of the ladder, respectively, and $\tilde{F}$ is the external linear force. $\tilde{g}$ is the strength of the interatomic interaction. In this paper, we take the case of $\tilde{g} > 0$, where the atoms repel each other. Experimentally, this ladder system can be readily realized by using a superlattice structure together with effective magnetic field (created by laser-assisted tunneling technology) in a two-dimensional optical lattice [12]. The rung-to-leg coupling ratio $\tilde{K}$ can be controlled by adjusting the intensity of the lasers which create the lattice potential, while the effective magnetic field ϕ can be turned by changing the wavelength of the running-wave beams or the angle between them. The external linear force $\tilde{F}$ can be realized by modulating the lattice potential [34]. To avoid parametric and interband excitations, weak linear force is considered, i.e., $\tilde{F}/\tilde{J} \ll 1$. The strength of the atomic interaction $\tilde{g}$ can be easily manipulated by the Feshbach resonance technology [35]. As shown in experiment [12], the values of these parameters can be adjusted in a wide range and $0 < \tilde{K}/\tilde{J} < 4$ and $0 < \phi < \pi$ are realized. The values of these parameters used in our work are all in experimental accessible range. This system is equivalent to a spin-orbit coupling system by regarding the left-right leg degree of freedom as a pseudospin.

Under the mean-field approximation, $a_{m,\sigma} = \langle \hat{a}_{m,\sigma} \rangle$ is the probability amplitude of atoms on the ladder leg at position m, and the Hamiltonian has the following form:

$$\begin{aligned}H = &-\tilde{J}\sum_m (e^{i\phi}a_{m,L}a^*_{m+1,L} + e^{-i\phi}a_{m,R}a^*_{m+1,R} + \text{H.c.}) \\ &- \tilde{K}\sum_m (a^*_{m,L}a_{m,R} + \text{H.c.}) + \frac{\tilde{g}}{2}\sum_m (|a_{m,L}|^4 + |a_{m,R}|^4) \\ &+ \tilde{F}\sum_m m(|a_{m,L}|^2 + |a_{m,R}|^2).\end{aligned} \tag{2}$$

In the meantime, according to the Heisenberg equation of motion ($i\hbar da_{m,\sigma}/dt = \partial H/\partial a^*_{m,\sigma}$), our system can be expressed by a set of discrete nonlinear Schrödinger equations:

$$\begin{aligned}i\dot{a}_{m,L} &= -(e^{-i\phi}a_{m+1,L} + e^{i\phi}a_{m-1,L}) - Ka_{m,R} \\ &\quad + g|a_{m,L}|^2 a_{m,L} + Fma_{m,L}, \\ i\dot{a}_{m,R} &= -(e^{i\phi}a_{m+1,R} + e^{-i\phi}a_{m-1,R}) - Ka_{m,L} \\ &\quad + g|a_{m,R}|^2 a_{m,R} + Fma_{m,R},\end{aligned} \tag{3}$$

where $\hbar = 1$, $K = \tilde{K}/\tilde{J}$, $g = \tilde{g}/\tilde{J}$, and $F = \tilde{F}/\tilde{J}$. Note that the time t is readjusted to $[\hbar/\tilde{J}]t$. They are dimensionless.

The ground-state and BOs dynamics of the system can be well studied by using a variational method. We use the Gaussion distribution of the wave packet with a radius R_σ,

$$a_{m,L}(t) = \sqrt{\frac{1+s}{2}}\frac{1}{R_L^{1/2}(\pi/2)^{1/4}} \times \exp\left[-\frac{(m-\xi_L)^2}{R_L^2} + ip_L(m-\xi_L) + i\frac{\theta}{2}\right],$$
$$a_{m,R}(t) = \sqrt{\frac{1-s}{2}}\frac{1}{R_R^{1/2}(\pi/2)^{1/4}} \times \exp\left[-\frac{(m-\xi_R)^2}{R_R^2} + ip_R(m-\xi_R) - i\frac{\theta}{2}\right], \quad (4)$$

where $\xi_\sigma(t)$ and $p_\sigma(t)$ represent the center-of-mass position and the related momentum in the corresponding legs, respectively. The degree of freedom of the left-right in the ladder can be considered a pseudospin. Hence, the parameters $\theta(t)$ and $s(t)$ represent, respectively, the phase difference and the spin population difference of atoms between the two legs of the ladder. The average spin polarization $\langle\sigma_z\rangle = s$ ranges from -1 to 1.

By means of variational method, the differential equation of motion can be obtained from the Lagrangian density $L = \sum_m \frac{i}{2}(\dot{a}_{m,L}a^*_{m,L} - a_{m,L}\dot{a}^*_{m,L} + \dot{a}_{m,R}a^*_{m,R} - a_{m,R}\dot{a}^*_{m,R}) - H$, the dot means the first derivatives with respect to t, and the asterisk means the complex conjugate. Specially, we assume $\xi_L = \xi_R = \xi$, $p_L = p_R = p$, $R_L = R_R = R$ to simplify the calculation and the sum over m in the Lagrangian density is replaced by an integral in the computational process. Under this circumstance and inserting Eq. (4) into the Lagrangian, we can get

$$L = p\dot{\xi} - \frac{1}{2}s\dot{\theta} + 2e^{-\frac{1}{2R^2}}(\cos p\cos\phi + s\sin p\sin\phi) + K\sqrt{1-s^2}\cos\theta - \frac{g(1+s^2)}{4\sqrt{\pi}R} - F\xi, \quad (5)$$

and the effective Hamiltonian is

$$H = -2e^{-\frac{1}{2R^2}}(\cos p\cos\phi + s\sin p\sin\phi) - K\sqrt{1-s^2}\cos\theta + \frac{g(1+s^2)}{4\sqrt{\pi}R} + F\xi. \quad (6)$$

Then we solve the Euler-Lagrangian equations $\frac{d}{dt}\frac{\partial}{\partial\dot{q}} = \frac{\partial L}{\partial q}$, and the differential equations of motion associated with the variational parameters $q(t) = \xi, p, \theta, s$ can be worked out

$$\dot{\xi} = 2e^{-\frac{1}{2R^2}}(\sin p\cos\phi - s\cos p\sin\phi), \quad (7)$$

$$\dot{p} = -F, \quad (8)$$

$$\dot{\theta} = -\frac{2Ks\cos\theta}{\sqrt{1-s^2}} + 4e^{-\frac{1}{2R^2}}\sin p\sin\phi - \frac{gs}{\sqrt{\pi}R}, \quad (9)$$

$$\dot{s} = 2K\sqrt{1-s^2}\sin\theta. \quad (10)$$

Equations (7) and (8) characterize the evolution of the center-of-mass position and the momentum of the condensate, respectively. That is, the BOs are controlled by Eqs. (7) and (8). The Eqs. (9) and (10) describe, in dynamic evolution, the change of the phase difference and the spin population difference between the two-leg ladder. In other words, the spin dynamics is characterized by the internal Josephson Eqs. (9) and (10). Equations (7)–(10) indicate that the BOs and spin dynamics are strongly coupled by the magnetic filed ϕ. In the next sections, we will study the ground-state transition and the BOs dynamics of the system.

III. THE GROUND-STATE TRANSITION WITHOUT TILT

First, we analytically study the ground state of the system in the absence of external linear force ($F = 0$) based on the variational equations. Equations (7)–(10) have the ground state q_0 when $F = 0$. We set that the center-of-mass position of the wave packets is at the origin of the coordinate, i.e., $\xi_0 = 0$. Meanwhile, using stationary solutions $\dot{q}_0 = 0$, we obtain $\theta_0 = 0$, $p_0 = \arctan(s_0\tan\phi)$, and

$$s_0 f = 0\left(f = -\frac{2K}{\sqrt{1-s_0^2}} + 4e^{-\frac{1}{2R^2}}\cos p_0\sin\phi\tan\phi - \frac{g}{\sqrt{\pi}R}\right). \quad (11)$$

Equation (11) determines the phase transition condition. $s_0 = 0$ means that $p_0 = 0$ and the distribution of particles in two legs is same, that is, the system is in the zero-momentum state. Additionally, $s_0 \neq 0$ (s_0 is determined by $f = 0$) means $p_0 \neq 0$ and the system is in the plane-wave state, where the particles are unevenly distributed in the two legs. Then, setting $s_0 = 0$ and $f = 0$, we get the critical condition of ground-state transition between the zero-momentum state and the plane-wave state,

$$K = 2e^{-\frac{1}{2R^2}}\sin\phi\tan\phi - \frac{g}{2\sqrt{\pi}R}, \quad (12)$$

which explicitly depicts the competition relationship among atomic interaction, magnetic field and rung-to-leg coupling ratio for inducing the ground-state transition. It can be clearly seen from Eq. (12) that atomic interaction g, rung-to-leg coupling ratio K and the magnetic filed ϕ can modify the ground state.

In the ground state, the energy of the system is described as follows:

$$H = -2e^{-\frac{1}{2R^2}}(\cos p\cos\phi + s\sin p\sin\phi) - K\sqrt{1-s^2} - \frac{g(1+s^2)}{4\sqrt{\pi}R}, \quad (13)$$

with the relationship of $p = \arctan(s\tan\phi)$. Then the dispersion relation of the band can be obtained. As the rung-to-leg coupling ratio K decreases, the band minimum shifts from $p_0 = 0$ to two nonzero p_0 values, and the two nonzero p_0 are degenerate and symmetric around $p_0 = 0$. The ground states of these two band structures correspond to the zero-momentum state and the plane-wave state, respectively. Figure 2 shows the energy spectra under different states for $g = 0.5$ and $g = 1.5$. It can be clearly seen that the energy

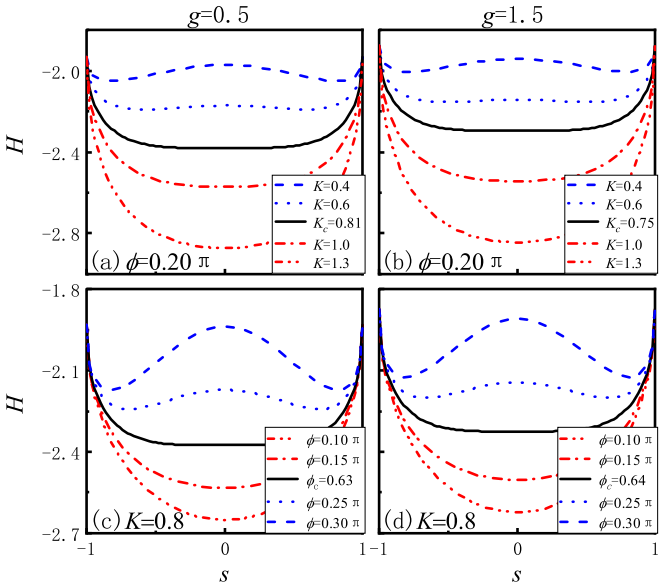

FIG. 2. Energy band structures of the ladder system under $g = 0.5$ (the left column) and $g = 1.5$ (the right column). The red line and blue line indicate that the ground state of the system is in the zero-momentum state and the plane-wave state, respectively. The black line is the energy spectrum at the transition point. We set $R = 5$.

spectra have a parabola structure with only one minimum in the zero-momentum state and the energy spectra have a double-well structure with two minimums in the plane-wave state. In addition, the energy band structure gradually transitions from the zero-momentum state to the plane-wave state with the decrease (increase) of $K(\phi)$.

The ground-state diagrams in K-g and ϕ-g planes for different ϕ and K are plotted in Fig. 3. It can be clearly seen that the transition from zero-momentum state to plane-wave state occurs with decreasing K, increasing ϕ or decreasing g. With the increase of g, the region of the zero-momentum state increases, indicating that the atomic interaction promotes the system to be in the zero-momentum state. In a word, the rung-to-leg coupling ratio$K$, magnetic flux ϕ, and the atomic

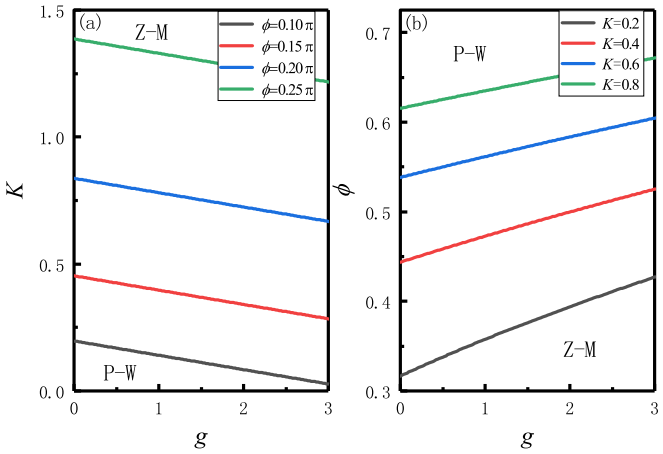

FIG. 3. The ground-state diagram in K-g plane under different ϕ (a) and in ϕ-g plane under different K (b).

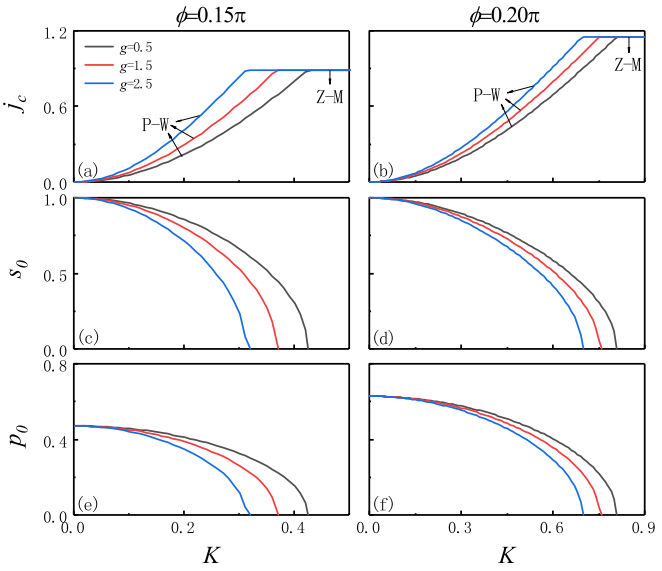

FIG. 4. The chiral current j_c, the initial spin population difference of atoms s_0 and the momentum p_0 corresponding to the ground state as function of the rung-to-leg coupling ratio K.

interacting g play important roles in the ground-state transition. Thus, we can control the ground state of the system by adjusting the strength of g, K, and ϕ.

In particular, we calculate the chiral currents, which can be observed experimentally and allow one to characterize the different ground state of the system [12]. We define the chiral current [36,37],

$$j_c = \sum_m (j_{m,L} - j_{m,R}) = 2e^{-\frac{1}{2R^2}}(s_0 \sin p_0 \cos\phi - \cos p_0 \sin\phi), \quad (14)$$

where the local currents on legs are $j_{m,\sigma} = i(e^{\pm i\phi} a^\dagger_{m+1,\sigma} a_{m,\sigma} - \text{H.c.})$.

Figure 4 shows the chiral current j_c, the initial population difference of atoms s_0 and the momentum p_0 corresponding to the ground state as a function of the rung-to-leg coupling ratio K to visualize the ground-state transition. As can be seen from Figs. 4(a) and 4(b), j_c increases with the increase of K in the plane-wave state until it reaches saturation in the zero-momentum state. The greater the magnetic flux ϕ is, the greater the saturated chiral current j_c is. It can be seen from Figs. 4(c)–4(f) that the density is higher on one leg than the other ($s_0 \neq 0$), and the momentum is nonzero ($p_0 \neq 0$) in the plane-wave state. In addition, the density is uniform ($s_0 = 0$), and the momentum is zero ($p_0 = 0$) in the zero-momentum state. The ground-state transition is a second-order-state transition because j_c, s_0, and p_0 are continuous across the boundary between the different states.

IV. THE CHIRAL BLOCH OSCILLATION AND SPIN DYNAMICS

When the bosonic ladder is tilted ($F \neq 0$), the system will not be in the ground state, causing interesting dynamics phenomena such as BOs of lattice system. Moreover, the features of the dynamics phenomena can directly differentiate

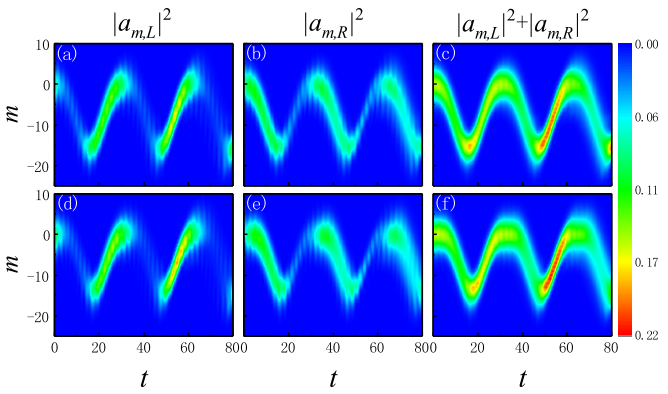

FIG. 5. Temporal evolutions of the left leg density (the first column), the right leg density (the second column) and the sum density (the third column) for oscillatory mode of a Gaussian wave packet in the zero-momentum state (the first row) and the plane-wave state (the second row). [(a)–(c)] With $\phi = 0.20\pi$; [(d)–(f)] with $\phi = 0.25\pi$. The other system parameters are $g = 0.5$, $K = 1.2$, and $F = 0.2$.

the novel state. In order to further elucidate the state transition of the magnetic ladder system, we study the BOs caused by a constant external force. We discuss the weak force case $F \ll 1$ to ensure that the characteristics of the ground state of the system are not affected strongly. Furthermore, it is known that strong repulsive atomic interaction can cause the decoherence of the condensates, which will result in damping of the BOs after a certain time. The damping rate is proportional to the strength of atomic interaction. So, to observe significant BOs in sufficiently long time, here we consider weak repulsive atomic interaction, i.e., $0 < g < 1$. This also is consistent with the experiment [12], where the strength of the atomic interaction can be easily manipulated by the Feshbach resonance technology. According to Eq. (8), the quasimomentum $p = p(t)$ satisfies the classical equation of motion,

$$p(t) = p_0 - Ft. \tag{15}$$

In this case, the external linear force plays the role of restoring force.

To survey the BOs started in different ground states, we have employed direct numerical simulations of the GP Eq. (3) using the fourth-order Runge-Kutta method. The results of the simulation for the cases started initially in different ground states are presented in Fig. 5.

As is shown, atoms exhibit the oscillatory mode of BOs. The chiral characteristics of the BOs are exhibited intuitively: When moving down (up) during the first (second) half of the BOs period, the particles are mainly distributed on the right (left) leg of the ladder. The degree of freedom of the left-right in the ladder is equivalent to pseudospin, and the different stages of the BOs period can be considered as different momenta [36]. That is, the spin-momentum locking results in the chirality of the system. On the other hand, comparing the first and second rows in Fig. 5, it can be seen that the BOs started in different ground states have dissimilar trajectories. Specifically, when the wave packet oscillates back to the initial site, it stays near the initial position for a longer time in the plane-wave state. Therefore, the oscillation characteristics

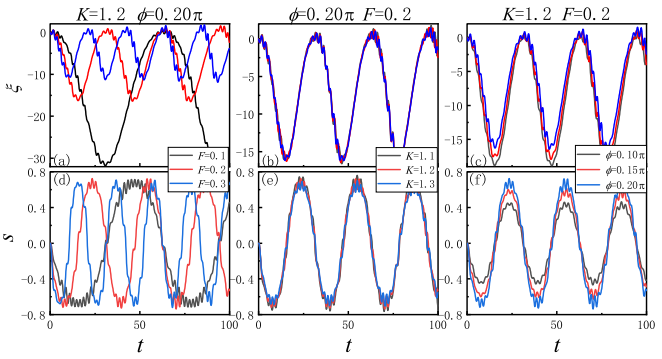

FIG. 6. The BOs and the spin dynamics in the regime of the zero-momentum state for $g = 0.5$ under different parameters F, K, and ϕ. [(a)–(c)] The temporal evolutions of the center of wave packets. [(d)–(f)] The temporal evolutions of the spin polarization.

of the magnetic ladder system can be used to distinguish the ground states of the system.

Instead, the BOs of the condensates are described by the dynamic of center-of-mass of wave packets ξ. Then we can obtain an equation describing the BOs by combining Eqs. (6)–(10),

$$\ddot{\xi} + F^2\xi = FH + F\left[K\cos\theta\sqrt{1-s^2} - \frac{g(1+s^2)}{4\sqrt{\pi}R}\right] - 2e^{-\frac{1}{2R^2}}\dot{s}\cos p\sin\phi. \tag{16}$$

It illustrates that the corresponding oscillatory period $T_B = 2\pi/F$. Equation (16) indicates that the BOs and the spin dynamics are strongly coupled in the presence of artificial magnetic flux. To obtain the amplitude of the BOs analytically, we solve the Eq. (7) approximatively. According to Figs. 6 and 7, we can assume $s(t) = \bar{s} = \int_0^{T_B} s(t)dt \approx 0$ when $\xi \to \xi_{\max}$, and then from Eq. (7), the maximal displacement $\xi_{\max}$ is obtained,

$$\xi_{\max} = -\frac{2e^{-\frac{1}{2R^2}}\cos\phi[1+\sin(p_0+\pi/2)]}{F}. \tag{17}$$

Equation (17) indicates that, the amplitude of the BOs is determined by F, p_0, and ϕ. Particularly, $\xi_{\max}$ depends on initial momentum $p_0 = \arctan(s_0\tan\phi)$, which means the amplitudes of BOs started in two ground states should be different.

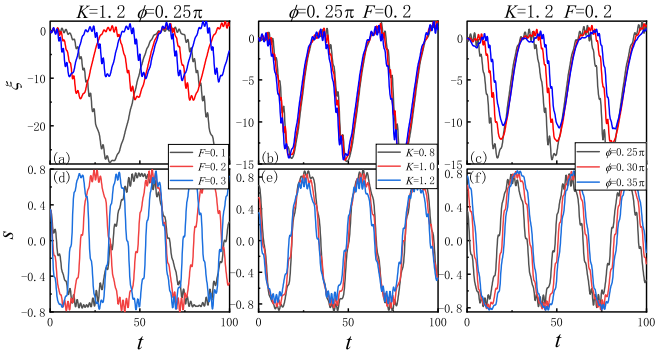

FIG. 7. The same as in Fig. 6 but in the regime of the plane-wave state.

The amplitude of BOs depends on K in the plane-wave state, while it does not in the zero-momentum state.

To reveal the BOs more clearly, we are interested in the evolution of the center-of-mass of wave packet, which can be characterized by its coordinate $\xi_\sigma(t)$ defined as $\xi_\sigma(t) = \int a^*_{m,\sigma} m a_{m,\sigma} dm / a^*_{m,\sigma} a_{m,\sigma} dm$. And we formulate the spin dynamics with $s(t) = \int (a^*_{m,L} a_{m,L} - a^*_{m,R} a_{m,R}) dm$, as displayed in Figs. 6 and 7. The results shown in Figs. 6 and 7 are the numerical solutions of Eq. (3), and only the center-of-mass of left leg ξ_L is shown. One can find that, because of the coupling of BOs and spin dynamics, the BOs and spin oscillation are all anharmonic. Whether the BOs is started in zero-momentum state (Fig. 6) or plane-wave state (Fig. 7), the frequencies of the BOs and spin oscillation indeed increase with the increasing F [see Figs. 6(a)–6(d) and Figs. 7(a)–7(d)], and the amplitudes of the BOs increase with the decrease of F and ϕ [see Figs. 6(a), 7(a) and Figs. 6(c), 7(c)], while they are independent of K in the zero-momentum state [see Fig. 6(b)] and have a weak dependence on K in the plane-wave state [see Fig. 7(b)] for fixed ϕ and F. The periodic spin dynamics is enhanced by the increase of ϕ [see Fig. 6(f) and Fig. 7(f)]. In particular, the influence of ϕ on s in the zero-momentum state is stronger than that in the plane-wave state. Interestingly, the amplitudes of s do not vary with F [see Fig. 6(d) and Fig. 7(d)], and K has very little impact on s [see Fig. 6(e) and Fig. 7(e)]. Those are all well predicted by Eq. (17). One can see more clearly that the centers of the Gaussian wave packets have different trajectories in two different ground states (see the first row in Figs. 6 and 7). Note that the numerical results in Figs. 6 and 7 show that ξ indeed approaches its maximum when $s \to 0$. This further confirm the validation of Eq. (17).

V. THE MODULATION OF BOs AND SPIN DYNAMICS

We turn to investigate the impact of a periodic modulation of the amplitude of the linear force on the dynamics of bosonic ladder. We consider a general harmonic force of the form $F(t) = F_0 \sin(\omega t + \varphi)$, where F_0 and φ are the amplitude and the initial phase, with frequency ω and period $T = 2\pi/\omega$. The variational equation of momentum (8) becomes

$$\dot{p} = -F_0 \sin(\omega t + \varphi). \tag{18}$$

By integrating the above formula, we get $p = p_0 + \frac{F_0}{\omega}[\cos(\omega t) - \cos\varphi]$. After inserting the integral result into Eq. (7), the dynamics of the wave-packet center is governed by the equation

$$\dot{\xi} = 2e^{-\frac{1}{2R^2}} \sqrt{\cos^2\phi + s^2 \sin^2\phi} \times \sin\left[\frac{F_0}{\omega}\cos(\omega t) - \frac{F_0}{\omega}\cos\varphi + p_0 - \arctan(s\tan\phi)\right]. \tag{19}$$

If the average velocity of the wave packet over a period T is zero, then the wave-packet shape is restored after each period, i.e., no dispersion occurs, then the condition should be satisfied when

$$\int_0^T \dot{\xi} dt = 0. \tag{20}$$

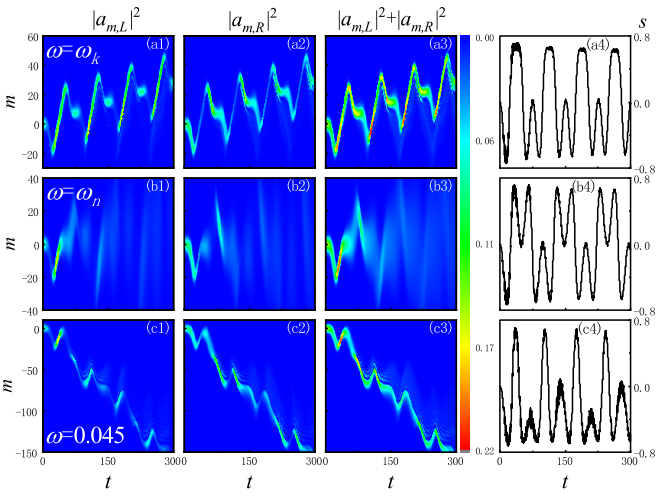

FIG. 8. Temporal evolutions of the left leg density (the first column), the right leg density (the second column) and the sum density (the third column) for oscillatory mode of a Gaussian wave packet in the zero-momentum state. The fourth column shows the corresponding time evolution of the spin polarization. The first row: $\omega = \omega_k = \frac{F_0}{\nu_1} = 0.0832$; the second row: $\omega = \omega_n = \frac{F_0}{\pi} = 0.0637$; the third row: $\omega = 0.0450$. The other system parameters are $g = 0.5$, $K = 1.2$, $\phi = 0.20\pi$, and $F_0 = 0.2$.

Actually, when Eq. (20) is satisfied, the dynamic localization occurs [38]. Now we also approximately assume $\int_0^T s(t)dt \approx 0$, and the integral in Eq. (20) is worked out in the condition

$$\sin\left(\frac{F_0}{\omega}\cos\varphi - p_0\right) \times J_0\left(\frac{F_0}{\omega}\right) = 0, \tag{21}$$

where $J_0(\cdot)$ is the zero-order Bessel function of the first kind. When Eq. (21) is satisfied, the resonant frequencies $\omega = \omega_k$ at which dynamic localization occurs can be found. Setting $J_0(\frac{F_0}{\omega}) = 0$, ω_k can be approximately provided by $\omega_k = \frac{F_0}{\nu}$, where $\nu_1 \approx 2.405$, $\nu_2 \approx 5.520$, etc., are zeros of $J_0(\nu)$. With the frequencies ω_k, the wave packet varies periodically in time, i.e., stable BOs occurs. The condition (21) is also satisfied at the case $\frac{F_0}{\omega}\cos\varphi - p_0 = n\pi$, i.e., $\omega = \omega_n = \frac{F_0\cos\varphi}{n\pi + p_0}$, where n is an integer. But these zeros reflect the adiabatic theorem [39] ensuring a change in the quasimomentum due to slowly changing weak external force. The zeros ω_n depend on the initial momentum p_0 and the initial phase of the external force φ, so the dynamics of the wave packets will be accompanied with the effective dispersion at $\omega = \omega_n$. Hence the frequencies ω_n do not represent authentic resonant frequencies corresponding to the dynamic localization, the resonances at $\omega = \omega_n$ will be set to pseudoresonances to isolate from $\omega = \omega_k$. Through calculation, it is found that there is always a pseudoresonance between two resonances, i.e., ω_k and ω_n alternate.

To confirm the results of the analytical predictions, we perform the direct numerical simulations of Eq. (3). For this purpose, we set $F_0 = 0.2$ and $\varphi = 0$, i.e.,

$$F(t) = F_0 \sin(\omega t). \tag{22}$$

In Figs. 8 and 9, the time evolution of the wave packets started from zero-momentum state (Fig. 8) and plane-wave state (Fig. 9) with different modulating frequencies of the

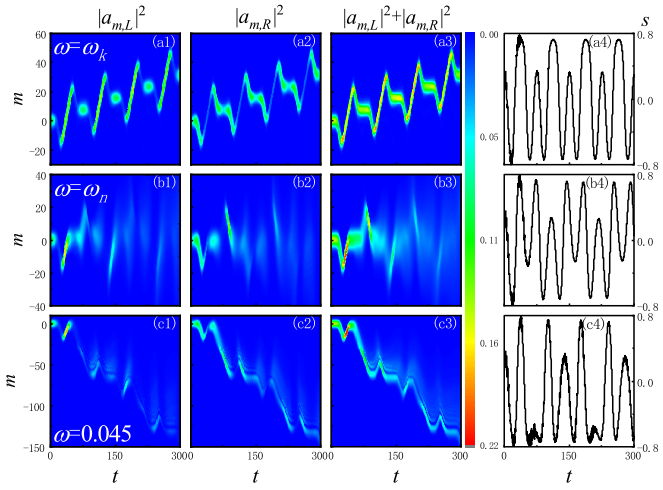

FIG. 9. The same as in Fig. 8 but in the regime of the plane-wave state with $g = 0.5$, $K = 1.2$, $\phi = 0.25\pi$, $F_0 = 0.2$, and $\omega_n = \frac{F_0}{\pi+p_0} = 0.0575$.

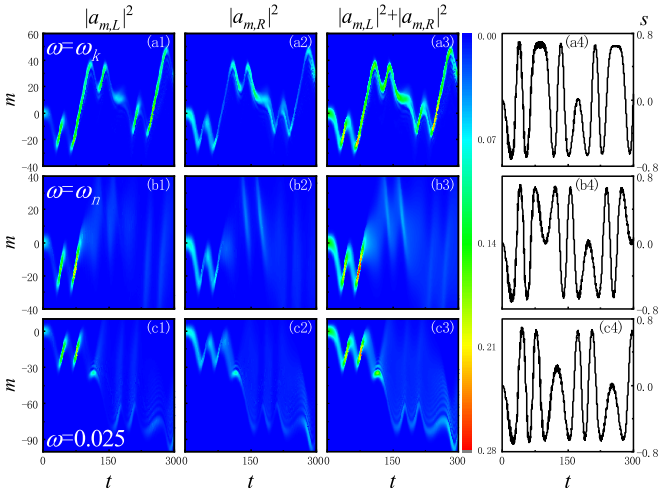

FIG. 10. Temporal evolutions of the left leg density (the first column), the right leg density (the second column) and the sum density (the third column) for oscillatory mode of a Gaussian wave packet in the zero-momentum state. The fourth column shows the corresponding time evolution of the spin polarization. The first row: $\omega = \omega_k = \frac{F_0}{\nu_2} = 0.0362$; the second row: $\omega = \omega_n = \frac{F_0}{2\pi} = 0.0318$; the third row: $\omega = 0.0250$. The other system parameters are $g = 0.5$, $K = 1.2$, $\phi = 0.20\pi$, and $F_0 = 0.2$.

linear force are shown. In Figs. 8 and 9, the first rows show the evolutions in the first resonance, i.e., $\omega = \omega_k = \frac{F_0}{\nu_1}$. It is clear that, there is no diffusion but weak drift in a resonance, i.e., stable BOs occurs. In this case, strong BOs with larger amplitude is observed. In a pseudoresonance (the second rows in Figs. 8 and 9), the wave packets have no drift, but we can see obvious diffusion, i.e., dispersion of wave packet takes place. The third rows in Figs. 8 and 9 show the considerable drift and the slow diffusion of the wave packets at nonresonant frequencies. The resonance frequency and pseudoresonance frequency obtained by analytical predictions are well confirmed by numerical simulations.

Importantly, the motion of the wave packet is also accompanied by periodic but anharmonic spin oscillations in all cases. As shown in the fourth columns in Figs. 8 and 9, the spin oscillations take different forms at different frequencies. Additionally, the duration of $s < 0$ is different from that of $s > 0$ in each oscillation period. Particularly, the duration of $s < 0$ is always longer than that of $s > 0$ at nonresonant frequencies [Fig. 8(c4) and Fig. 9(c4)]. In the resonances cases [Fig. 8(a4) and Fig. 9(a4)], the duration of $s < 0$ is longer in the zero-momentum state, but in the plane-wave state the situation is completely reversed. Because of the spin-momentum locking, the features of spin evolution have a direct effect on the oscillation of wave packet. Compared with Fig. 5, we find the chirality of BOs in the presence of periodic modulation (Fig. 8 and Fig. 9) is obviously different from that of conventional BOs (Fig. 5): during the oscillation, the particles are always mainly distributed on one (left or right) leg of the ladder, but the particles mainly occupy the right (left) leg for more time than the left (right) leg in the zero-momentum (plane-wave) state in one period. Moreover, like conventional BOs, the wave packet oscillates back to near its initial position and stay here longer in the plane-wave state than in the zero-momentum state after a period, too.

Figures 10 and 11 show the evolutions in the second resonance (i.e., $\omega = \omega_k = \frac{F_0}{\nu_2}$) and pseudoresonance (i.e., $\omega_n = \frac{F_0}{2\pi+p_0}$) and the drift of the wave packet at a smaller nonresonant frequency. As shown in the figures, the smaller the modulating frequency is, the more complex the spin dynamics is. Indeed, the corresponding oscillatory mode is also more complex. Interestingly, the direction of motion of the wave packet changes more times in one oscillatory period. Because the drift of the wave packet is accompanied by oscillation, this results in the fact that the wave packet drags more slowly at a smaller nonresonant frequency [see Figs. 10(c1)–11(c3) and Figs. 11(c1)–11(c3)]. Those results are obviously different from the results shown in Figs. 8 and 9 for the first resonances. The BOs, the wave-packet dynamics and the

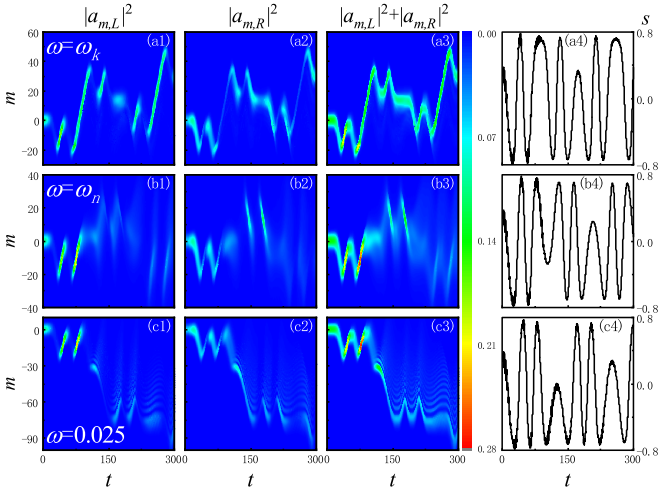

FIG. 11. The same as in Fig. 10 but in the regime of the plane-wave state with $g = 0.5$, $K = 1.2$, $\phi = 0.25\pi$, $F_0 = 0.2$, and $\omega = \omega_n = \frac{F_0}{2\pi+p_0} = 0.0302$.

corresponding spin dynamics can be well controlled by the periodic modulation of the external force.

Note that the Bloch dynamics considered in our work is at zero temperature. However, real experiment is always at finite temperature. The Bloch dynamics considered in our work is based on the ground state of the system. Because of thermal fluctuations, the ground-state phases and the coherent Bloch dynamics will be destroyed as temperature increases. Finite temperature has a blurring effect on the ground-state phases [40,41]. However, it is shown that [40,41], at finite temperature T and when $T/J < 1$, the ground-state phases obtained at zero temperature can still be clearly resolved. This condition can be well satisfied by the current experiment [12], where, the distinct ground-state phases are observed at finite temperature. Furthermore, in studying the Bloch dynamics, we consider weak external force, i.e., $F \ll 1$, then, parametric and interband excitations are avoided safely and the characteristics of the ground state of the system are not affected strongly. Hence, the Bloch dynamics predicted in our work should be readily observed in current experiment.

VI. CONCLUSION

In conclusion, based on the variational method and numerical simulation, we have studied the Bloch dynamics and its modulation in bosonic ladder with magnetic flux. In the absence of the external linear force, we investigate the quantum-state transition of the system. The energy spectrum, chiral current diagram and ground-state diagram in the parameter space which clearly reflect the state transition process of the system are provided. The BOs in the magnetic ladder exhibit chiral characteristics under the action of an external linear force. The coupling of the linear force, artificial magnetic field, the rung-to-leg coupling ratio of the ladder results in rich BOs and spin dynamics. In addition, we discuss the effects of a time-periodic modulation of the amplitude of the linear force on the dynamics of bosonic ladder. The Bloch wave-packet dynamics in authentic resonances, pseudoresonances, and nonresonances are studied. The motion of Bloch wave packet presents rich features, and the oscillations are accompanied by anharmonic pseudospin dynamics in all cases. Compared with traditional Bloch oscillations under a static linear force, dynamic localization under a periodically modulated linear force offers more opportunities for controlling the particle dynamics. Indeed, it allows changing the law of motion of the particles simply in ladder system by varying the frequency of the linear force.

ACKNOWLEDGMENTS

This work is supported by the National Natural Science Foundation of China under Grants No. 12264045, No. 12164042, No. 11764039, No. 11847304, and No. 11865014; by Natural Science Foundation of Gansu Province under Grant No. 17JR5RA07620JR5RA526; by Scientific research project of Gansu higher education under Grand No. 2016A-005; by Innovation capability enhancement project of Gansu higher education under Grants No. 2020A-146 and No. 2019A-014; and by Creation of science and technology of Northwest Normal University under Grant No. NWNU-LKQN-18-33.

[1] J. Dalibard, F. Gerbier, G. Juzeliunas, and P. Öhberg, Rev. Mod. Phys. **83**, 1523 (2011).
[2] Y.-J. Lin, R. L. Compton, K. Jiménez-García, W. D. Phillips, J. V. Porto, and I. B. Spielman, Nat. Phys. **7**, 531 (2011).
[3] Y.-J. Lin, R. L. Compton, K. Jiménez-García, J. V. Porto, and I. B. Spielman, Nature (Lond.) **462**, 628 (2009).
[4] Y.-J. Lin, K. Jiménez-García, and I. B. Spielman, Nature (Lond.) **471**, 83 (2011).
[5] G. Gligorić, A. Maluckov, L. Hadžievski, Sergej Flach, and Boris A. Malomed, Phys. Rev. B **94**, 144302 (2016).
[6] S. Gautam and S. K. Adhikari, Phys. Rev. A **90**, 043619 (2014).
[7] C. Hamner, Yongping Zhang, M. A. Khamehchi, Matthew J. Davis, and P. Engels, Phys. Rev. Lett. **114**, 070401 (2015).
[8] Y. Zhang, Y. Xu, and T. Busch, Phys. Rev. A **91**, 043629 (2015).
[9] Y. Zhang and C. Zhang, Phys. Rev. A **87**, 023611 (2013).
[10] F. K. Abdullaev and M. Salerno, Phys. Rev. A **98**, 053606 (2018).
[11] Y. V. Kartashov, V. V. Konotop, D. A. Zezyulin, and L. Torner, Phys. Rev. Lett. **117**, 215301 (2016).
[12] M. Atala, M. Aidelsburger, M. Lohse, J. T. Barreiro, B. Paredes, and I. Bloch, Nat. Phys. **10**, 588 (2014).
[13] M. E. Tai, A. Lukin, M. Rispoli, R. Schittko, T. Menke, D. Borgnia, P. M. Preiss, F. Grusdt, A. M. Kaufman, and M. Greiner, Nature (Lond.) **546**, 519 (2017).
[14] F. A. An, E. J. Meier, and B. Gadway, Sci. Adv. **3**, e1602685 (2017).
[15] A. Dhar, T. Mishra, M. Maji, R. V. Pai, S. Mukerjee, and A. Paramekanti, Phys. Rev. B **87**, 174501 (2013).
[16] R. Wei and E. J. Mueller, Phys. Rev. A **89**, 063617 (2014).
[17] S. Uchino and A. Tokuno, Phys. Rev. A **92**, 013625 (2015).
[18] M. Piraud, F. Heidrich-Meisner, I. P. McCulloch, S. Greschner, T. Vekua, and U. Schollwöck, Phys. Rev. B **91**, 140406(R) (2015).
[19] S. Greschner, M. Piraud, F. Heidrich-Meisner, I. P. McCulloch, U. Schollwöck, and T. Vekua, Phys. Rev. A **94**, 063628 (2016).
[20] A. Keleş and M. Ö. Oktel, Phys. Rev. A **91**, 013629 (2015).
[21] E. Orignac, R. Citro, M. D. Dio, S. D. Palo, and M.-L. Chiofalo, New J. Phys. **18**, 055017 (2016).
[22] R. Khomeriki and S. Flach, Phys. Rev. Lett. **116**, 245301 (2016).
[23] T. Hartmann, F. Keck, H. J. Korsch, and S. Mossmann, New J. Phys. **6**, 2 (2004).
[24] Y.-J. Zhao, X.-W. Xu, H. Wang, Y.-X. Liu, and W.-M. Liu, Phys. Rev. A **102**, 053722 (2020).
[25] W. Tschischik, R. Moessner, and M. Haque, Phys. Rev. A **92**, 023845 (2015).
[26] Y. Zheng, S. Feng, and S.-J. Yang, Phys. Rev. A **96**, 063613 (2017).
[27] S. Liang, Z.-C. Li, W. Zhang, L. Zhou, and Z. Lan, Phys. Rev. A **102**, 033332 (2020).

[28] Y. Jian, X. Qiao, J.-C. Liang, Z.-F. Yu, A.-X. Zhang, and J.-K. Xue, Phys. Rev. E **104**, 024212 (2021).
[29] X. Qiao, X.-B. Zhang, Y. Jian, A.-X. Zhang, Z.-F. Yu, and J.-K. Xue, Phys. Rev. A **104**, 053323 (2021); X. Qiao, X.-B. Zhang, Y. Jian, A.-X. Zhang, and J.-K. Xue, Physica A **576**, 126062 (2021).
[30] A.-X. Zhang, L.-X. Cai, S.-Q. He, Z. Yu, X. Qiao, Y. Zhang, and J.-K. Xue, Europhys. Lett. **127**, 50007 (2019).
[31] D. Jaksch, V. Venturi, J. I. Cirac, C. J. Williams, and P. Zoller, Phys. Rev. Lett. **89**, 040402 (2002).
[32] M. Yan, H.-Y. Hui, M. Rigol, and V. W. Scarola, Phys. Rev. Lett. **119**, 073002 (2017).
[33] M. Yan, H.-Y. Hui, and V. W. Scarola, Phys. Rev. A **95**, 053624 (2017).
[34] K. Wintersperger, M. Bukov, J. Näger, S. Lellouch, E. Demler, U. Schneider, I. Bloch, N. Goldman, and M. Aidelsburger, Phys. Rev. X **10**, 011030 (2020).
[35] L.-C. Ha, C.-L. Hung, X. Zhang, U. Eismann, S.-K. Tung, and C. Chin, Phys. Rev. Lett. **110**, 145302 (2013).
[36] D. Hügel and B. Paredes, Phys. Rev. A **89**, 023619 (2014).
[37] S. Uchino, Phys. Rev. A **93**, 053629 (2016).
[38] D. H. Dunlap and V. M. Kenkre, Phys. Rev. B **34**, 3625 (1986).
[39] M. Born and V. A. Fock, Z. Phys. A **51**, 165 (1928).
[40] M. Buser, F. Heidrich-Meisner, and U. Schollwöck, Phys. Rev. A **99**, 053601 (2019).
[41] S. Greschner, M. Piraud, F. Heidrich-Meisner, I. P. McCulloch, U. Schollwöck, and T. Vekua, Phys. Rev. Lett. **115**, 190402 (2015).